

Dynamics of Airfoil Separation Control Using Zero-Net Mass-Flux Forcing

Reni Raju* and Rajat Mittal†

The George Washington University, Washington, D.C. 20052

and

Louis Cattafesta‡

University of Florida, Gainesville, Florida 32611

DOI: 10.2514/1.37147

Zero-net mass-flux jet based control of flow separation over a stalled airfoil is examined using numerical simulations. Two-dimensional simulations are carried out for a NACA 4418 airfoil at a chord Reynolds number of 40,000 and angle of attack of 18 deg. Results for the uncontrolled flow indicate the presence of three distinct natural time scales in the flow corresponding to the shear layer, separation bubble, and wake regions. The natural frequencies are used to select appropriate forcing frequencies, and it is found that forcing frequencies closer to the separation bubble frequency elicit the best response in terms of reduction of separation extent and an improvement in aerodynamic performance. In contrast, higher forcing frequencies closer to the natural shear layer frequency tend to enhance separation. The vortex dynamics and frequency response of flow are examined in detail to gain insight into mechanisms underlying the observed behavior.

I. Introduction

BOUNDARY layer control can significantly improve the aerodynamic performance of lifting bodies while increasing the range of pre-stall angle of attack. Controlling and modifying the inherent instabilities in the boundary layer is a means of effective flow control, and one way to achieve this is through periodic excitation [1–3]. Periodic forcing using zero-net mass-flux actuation can either control/delay boundary layer separation or lead to global modification of the flow to generate lift while reducing drag [2,4–7]. It is generally understood that the periodic entrainment and expulsion of the outer fluid, resulting from enhanced vortex formation, leads to a periodic addition of momentum or cyclic oscillations to a separating boundary layer, thereby improving its ability to overcome an adverse pressure gradient [8]. Studies show that these devices improve aerodynamic performance with significantly less addition of momentum as compared to steady blowing [2].

It is known that the key control parameters for sinusoidal excitation are the jet frequency f_j and jet velocity V_j (which is usually characterized by either the peak or rms jet velocity during the expulsion phase of a cycle). Several past studies have targeted key issues such as effective forcing frequencies [2,5,9,10] and momentum coefficient [2,5,6], which are of course dependent on the above control parameters. In addition, researchers have also investigated parameters such as actuator waveforms [10–12] and placement [2,6], relative direction [13], vorticity flux [14], and curvature effects [15]. Control authority varies monotonically with the ratio of jet velocity to freestream velocity V_j/U_∞ up to a point where a further increase completely disrupts the boundary layer. The effectiveness of the forcing can also be improved by placing the jet just upstream of the separation point [6]. In contrast to the jet

velocity, however, control authority has a highly nonmonotonic variation with dimensionless frequency $F^+ = f_j/f_n$, where f_n is some natural frequency in the baseline uncontrolled flow. In the past, f_n was usually assumed to be associated with the time scale of the separation region [2,11]. However, studies have found a large range of F^+ values that provide effective control [16]. This suggests that there is more than one natural time scale in these flows and that all of the physical mechanisms governing zero-net mass-flux (ZNMF)-based separation control are not yet fully understood.

As pointed out by Mittal and Kotapati [16], depending on flow conditions, there are at least three natural frequencies occurring in a separated airfoil flow. Typically at low angles of incidence, where the flow remains attached to the airfoil, only the global instability causing Kármán vortex shedding exists with a characteristic frequency f_{wake} . At higher angles of incidence due to the presence of an adverse pressure gradient, separation may occur and the flow may or may not reattach. In the latter case, there are at least two natural frequencies, f_{wake} and f_{shear} , and the latter is due to the Kelvin–Helmholtz-type instability of the separated boundary layer. On the other hand, if the flow does reattach before the trailing edge, a third frequency scale f_{sep} , corresponding to the separation bubble, may also be present. This frequency is associated with the periodic release of vortices from the separation region.

Each of the above frequency scales is governed by distinct scaling laws. The wake frequency scales as $f_{\text{wake}} \sim U_{\text{wake}}/W_{\text{wake}}$ [17], where U_{wake} is the flow velocity outside the wake and W_{wake} is the characteristic width of the wake. Similarly, the separation bubble frequency scales as $f_{\text{sep}} \sim U_\infty/L_{\text{sep}}$, where L_{sep} is the length of the separation bubble. The shear layer, if it evolves away from the influence of a wall, scales as \tilde{U}/θ [18], where \tilde{U} is the average velocity in the shear layer and θ is the momentum thickness just upstream of separation. However, in situations where the shear layer separates and reattaches there might be lock on of f_{shear} to f_{sep} through subharmonic resonance [19]. It is therefore plausible to hypothesize that the optimal forcing frequency, defined as the frequency that minimizes the extent of the flow separation region, depends on these three characteristic frequencies, $(f_j)_{\text{optimal}} = fn(f_{\text{shear}}, f_{\text{sep}}, f_{\text{wake}})$.

The question therefore remains as to which frequency or frequencies determine the most effective jet frequency and what is (are) the underlying physical mechanism(s) responsible for this. Mittal and Kotapati [16] reviewed the possibility of a wide range of optimal values of F^+ based on the various definitions used by

Received 19 February 2008; revision received 21 July 2008; accepted for publication 21 July 2008. Copyright © 2008 by the authors. Published by the American Institute of Aeronautics and Astronautics, Inc., with permission. Copies of this paper may be made for personal or internal use, on condition that the copier pay the \$10.00 per-copy fee to the Copyright Clearance Center, Inc., 222 Rosewood Drive, Danvers, MA 01923; include the code 0001-1452/08 \$10.00 in correspondence with the CCC.

*Graduate Student, Department of Mechanical and Aerospace Engineering, Student Member AIAA.

†Professor, Department of Mechanical and Aerospace Engineering; mittal@gwu.edu. Associate Fellow AIAA.

‡Professor, Interdisciplinary Microsystems Group, Department of Mechanical and Aerospace Engineering. Associate Fellow AIAA.

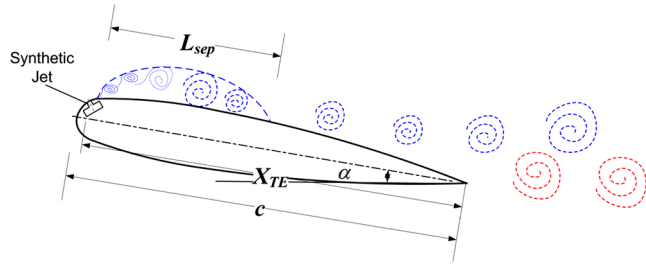


Fig. 1 Schematic showing the length scales used to identify the dimensionless frequency F^+ .

researchers. Note that F^+ is equivalent to a Strouhal number when defined as $F^+ = f_j l_c / U_\infty = St$, where l_c is an appropriate length scale in the flow configuration. Studies show that for $l_c = c$, the chord length, optimal values range from 0.55 to 5.5 [20–26]. For $l_c = X_{TE}$, the distance from the actuator to the trailing edge, this range is found to be 0.5 to 2.0 [5,27,28], while for $l_c = L_{sep}$ optimal values range from 0.75 to 2.0 [2,11,29].

Figure 1 shows a schematic of the aforementioned length scales for a generic airfoil. In general, $F^+ \sim \mathcal{O}(1)$ is found to provide effective flow control. However, in certain cases $F^+ \sim \mathcal{O}(10)$ has also shown to result in improved aerodynamics performance [6]. In contrast to the above studies, Wu et al. [9] argued that for poststall cases, the optimal control frequency should be a harmonic of f_{wake} . Because of the ability of the shear layer to respond to a broad range of frequencies a suitable choice for F^+ can allow both the vortex shedding and shear layer to lock on to the forcing frequency or its superharmonics. Hence there is still a need for further investigation of the nonlinear interactions of natural instabilities to the forcing frequency. Mittal and Kotapati [16], Mittal et al. [30], and Kotapati et al. [31] presented a novel configuration for investigating flows with these three distinct frequency scales, which consists of a separated flow over a thick elliptic plate. In their studies, it was found that forcing the jet at f_{sep} provided the most effective means of suppressing separation, with the shear layer and separation zone locking on to the forcing frequency or its subharmonic. On the other hand, when forcing was provided at frequencies higher than that of the shear layer, no improvement in separation control was obtained.

The shear layer instabilities of a flow over an airfoil during incipient stall are likely to be highly receptive to forcing, and in the present work we examine these issues for a conventional separated airfoil flow. The primary focus is to examine in detail the flow physics associated with stall and its response to the forcing at different frequencies. For this purpose we have chosen a 2-D NACA 4418 airfoil for which experimental drag data are available from Zaman and Culley [32]. They examined the effect of forcing frequency and velocity amplitude for a single jet location on poststall cases at high angles of attack. In the present work we have chosen a poststall case at a moderately high angle of attack α of 18 deg where the separated flow exhibits reattachment. This flow does indeed contain all three characteristic frequencies and thus permits an examination of the complex nonlinear vortex dynamics of the baseline and forced flow. To accomplish this, flow control is investigated over a range of frequencies, and the effects of two distinct jet locations are also investigated.

II. Simulation Overview

The simulations employ a sharp interface immersed boundary method (IBM) developed by Ghias et al. [33,34]. The method allows for simulation of compressible flow with immersed bodies on body nonconformal grids. The governing equations used are the unsteady, viscous, compressible Navier–Stokes equations written in terms of conservative variables. The equations are transformed to a generalized curvilinear coordinate system, while maintaining the strong conservation form of the equations [35]. They are discretized in the computational domain with a cell-centered arrangement using a hybrid, second-order central-difference quadratic upwind

interpolation for convective kinematics (QUICK) scheme [36], which allows for precise control of the numerical dissipation. The diagonal viscous terms are treated implicitly using a Crank–Nicolson scheme wherein all the other terms including the convective terms and cross terms are treated explicitly using a low-storage, third-order Runge–Kutta scheme [37]. Use of this mixed implicit–explicit scheme virtually eliminates the viscous stability constraint which can be quite severe in simulation of viscous flows. The resulting equations are solved by a line successive overrelaxation iterative method [35]. The IBM method is used to simulate flow past an immersed boundary on structured curvilinear grids that does not conform to the shape of the boundary and allows us to simulate the airfoil flow on a single-block mesh with no branch cuts. This topology maintains good grid quality in the entire domain. Validation and accuracy tests of this solver against experiments and numerical simulations have been presented elsewhere [33,34].

The 2-D airfoil configuration chosen for the current study is shown in Fig. 2. The airfoil is a NACA 4418 section similar to the experimental setup of Zaman and Culley [32]. The chord Reynolds number based on the freestream velocity is $Re_c = 40,000$, which matches the experiment. The current simulations are carried out on a nominal 386×158 grid on a domain size $7c \times 8c$. Figure 3 shows the curvilinear grid topology used for the current study. The free-stream velocity U_∞ is prescribed at the inflow, whereas a non-reflecting boundary condition is used at the exit that allows the vortex structures to be convected out with minimal spurious reflections. Slip boundary conditions are prescribed at the top and bottom walls which are placed at a sufficient distance from the airfoil surface.

For the control cases, the ZNMF actuator is modeled by providing an oscillatory boundary condition on the airfoil surface at a distance $x^+ = x_j/c$ from the leading edge of the form $V_j(t) = V_0 \sin(2\pi f_j^+ t)$, where V_0 is the amplitude and $f_j^+ = f_j c / U_\infty$ is the

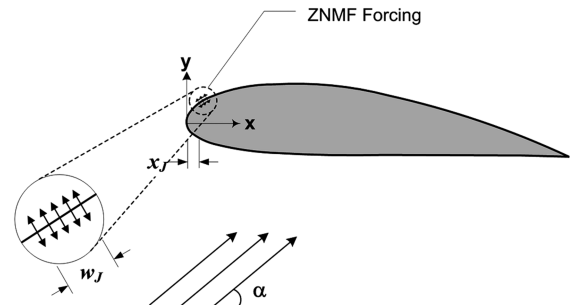


Fig. 2 Schematic of the airfoil configuration.

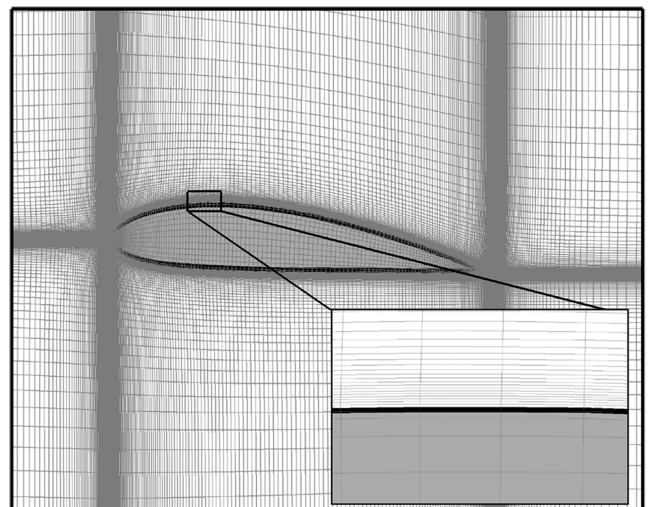


Fig. 3 Topology of the grid used in current simulation with grid size of 384×157 .

Table 1 Forcing parameters and response of the forced cases

Case	f_j^+	x_j^+	w_j^+	Response type	$\Delta C_l/C_l, \%$	$\Delta C_d/C_d, \%$	$\frac{\Delta(C_l/C_d)}{(C_l/C_d)}, \%$
1	0.5			I	8	13	-5
2	1.0 ($=f_{\text{wake}}^+$)				10	-28	52
3	1.5				4	-34	58
4	2.0 ($\approx f_{\text{sep}}^+$)			II	1	-39	64
5	3.0	0.024	0.012		5	-35	60
6	4.0				5	-34	59
7	6.0				7	-7	15
8	8.0				4	28	-19
9	10.0			III	-4	30	-27
10	12.0 ($\approx f_{\text{sl}}^+$)				-8	39	-34
11	2.0			—	-4	-24	27
12	10.0	0.070	0.019	—	1	21	-17

forcing frequency. The forcing is provided over a jet width $w^+ = w_j/c$ along the airfoil surface, which is equivalent to five grid points for the nominal grid. It should be mentioned here that the current method is only an approximation of a synthetic jet. However, including the cavity and slot in the simulations adds significantly to the overall computational cost due to the high resolution required to resolve the internal flow dynamics. Parallel work is being carried out in this regard to develop reduced order models which can accurately represent the characteristics of a synthetic jet [14,38,39]. Because the focus of the current study is to investigate the effect of forcing frequency on the nonlinear flow dynamics and we are not modeling any particular actuator, the very basic, top-hat representation of the ZNMF jet is chosen. A similar methodology was also adopted by Wu et al. [9] and such approximation has also been used by others in the past [40]. It should be noted, however, that the precise effect of modeling the actuator flow on flow control is not fully understood and this needs to be taken into account while interpreting the quantitative results of the study. All the flow-control simulations are based on a baseline flow configuration at an angle of attack, $\alpha = 18$ deg. A summary of the cases is listed in Table 1. Each simulation typically requires about 60–70 h of CPU time on a 20 processor Intel@Xeon computer.

Sensitivity of the results to the grid and domain has also been examined for the baseline case. Grid dependence studies where the flow is simulated on a finer 497×218 grid, such that resolution around the airfoil is nearly twice that of the nominal grid, show that the mean lift variation changes by less than 1% while the mean drag is within 4% of the value computed on the nominal grid. Increasing the total domain size by 75% showed that the variation in mean drag and lift were within 4.5% and 3%, respectively. Further details of these studies can be found in [41]. As will be discussed in the next section, the computed results are also compared with experimental data to further establish the fidelity of the current simulation setup.

III. Results

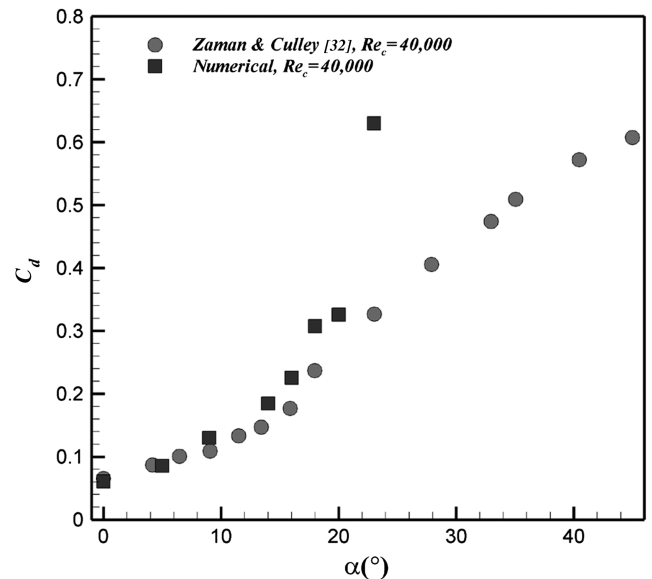
A. Baseline Uncontrolled Case

The focus of the current study is to examine separation control over a stalled airfoil. As a first step, two-dimensional simulations of flow over the NACA 4418 airfoil have been carried out over a range of angles of attack and the computed drag coefficients are compared to the experimental results [32]. The results, which are shown in Fig. 4, indicate that the 2-D simulations lead to a reasonable prediction of the drag coefficients up to $\alpha = 20$ deg. For higher angles, the 2-D calculations tend to overpredict the drag indicating the presence of strong three-dimensional effects in the experimental flow [42]. Comparison of the lift coefficients at different α indicates that the airfoil begins to stall for $\alpha > 16$ deg. Based on these results, the $\alpha = 18$ deg case is chosen as the baseline case for investigation of separation control. The advantage of choosing this case is that it affords an opportunity to examine the control of separation of a stalled airfoil using affordable 2-D numerical simulations.

Figure 5 shows the instantaneous spanwise vorticity plot at four different instants for the baseline uncontrolled case during one

convective time interval over the airfoil. At this angle of attack, the presence of an adverse pressure gradient causes the boundary layer to separate near the leading edge. The plots show the presence of two shear layers, one near the point of separation and the other at the trailing edge. The leading-edge shear layer undergoes a Kelvin–Helmholtz-type instability and rolls up into small clockwise rotating vortices. These vortices merge due to the deceleration of the fluid beyond the point of separation and form larger clockwise vortices which eventually release from the separation region and convect downstream. It should be noted that the shear layer undergoing separation is unsteady and hence the separation point is not fixed. At the trailing edge, the pressure side boundary layer separates and rolls up into counterclockwise vortices which, together with the clockwise vortices from the suction side, form the “wake” of the airfoil. Defining the edge of the wake to be where the mean velocity reaches 99% of U_∞ , the width of the wake at half-chord distance downstream of the trailing edge is found to be approximately $0.85c$. The time-averaged streamlines shown in Fig. 6 give some idea of the extent of separation. The flow separates near the leading edge of the airfoil at about $x^+ = 0.032$ and reattaches in the mean at about $x^+ = 0.75$, where $x^+ = x/c$. The separation bubble formed due to the adverse pressure gradient therefore has an approximate length, $L_{\text{sep}} \sim 0.72c$ and height, $H_{\text{sep}} \sim 0.07c$. Furthermore, as shown in the inset, a secondary recirculation region is also formed and it extends from $x^+ \sim 0.09$ to 0.26 .

To gain insight into the time scales associated with the various features of this flow, we examine the temporal variation of the


Fig. 4 Variation of drag coefficient as a function of α compared with experimental data.

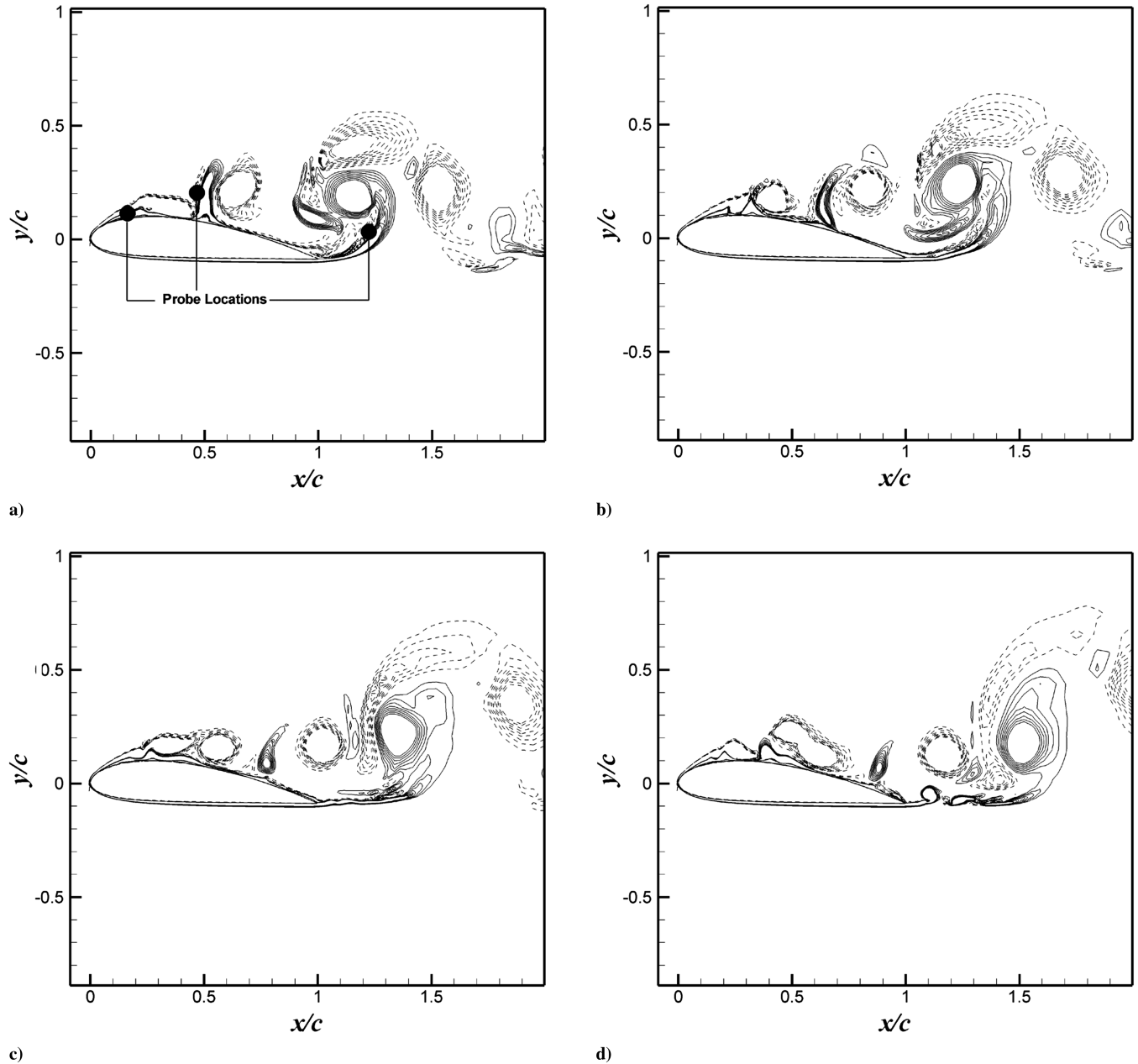


Fig. 5 Transient instantaneous uncontrolled flow over one convective time interval, $t/T = 0$ a), 0.25 b), 0.5 c), and 0.75 d). Dashed and solid lines represent clockwise and counterclockwise vorticity.

cross-stream velocity at three locations indicated by circles in Fig. 5a. The streamwise locations of these probes are $x^+ = 0.14$, $x^+ = 0.46$, and $x^+ = 1.22$, which correspond to the regions influenced by the shear layer, separated vortices, and wake, respectively. Figure 7a shows the temporal variation of the cross-stream velocity corresponding to the shear layer and it can be seen that due to the highly stochastic nature of the flow, the corresponding power spectrum, shown in Fig. 7b, cannot clearly identify a dominant frequency in this region. For this reason we use a two-step approach for identifying the characteristic frequency in a particular region. The first method identifies the dominant frequency range using a probability density function (PDF) approach, and the second method averages the windowed power spectra to reduce the random variations in the spectrum.

In the PDF-based approach, the consecutive maxima and minima in the temporal variation of the cross-stream velocity temporal variation shown in Fig. 7a are first identified. Once these peaks and troughs are known, the time intervals $\Delta\tau$ between all consecutive maxima and all consecutive minima are calculated for the whole time series. We now associate a nondimensional oscillation frequency

with each of these time intervals as $f_{PDF}^+ = c/(U_\infty \Delta\tau)$, resulting in a distribution of f_{PDF}^+ . Using a built-in function (*dfttool*) in MATLAB®, the PDF of these frequencies is calculated as shown in Fig. 7c. Based on this estimate, the most probable frequency of oscillation is estimated. Note that this method deemphasizes the cycle-to-cycle changes in amplitude and works well for the relatively complex temporal variation that is observed here. The nonparametric fit of the probability density function estimates the most probable frequency in the shear layer to be $f_{PDF}^+ = 11.3$.

The second method divides the time series into a number of overlapping windows (window size $tU_\infty/c = 1$ with 50% overlap) and the average power spectrum is recalculated using the fast Fourier transform for all these windows. The time series contains 14,000 points with $\Delta t U_\infty/c = 0.0002$, resulting in more than 50 windows for each case. The resulting power spectrum (Fig. 7d) indicates that $f_{shear}^+ \approx 12.0$, where $f^+ = fc/U_\infty$. The spectrum also shows a larger peak at $f^+ \approx 5$, but this frequency is related to subharmonics and/or lower-frequency modulations of the shear layer due to the separation bubble. Note that the instantaneous spectrum in Fig. 7b also shows a peak at this frequency.

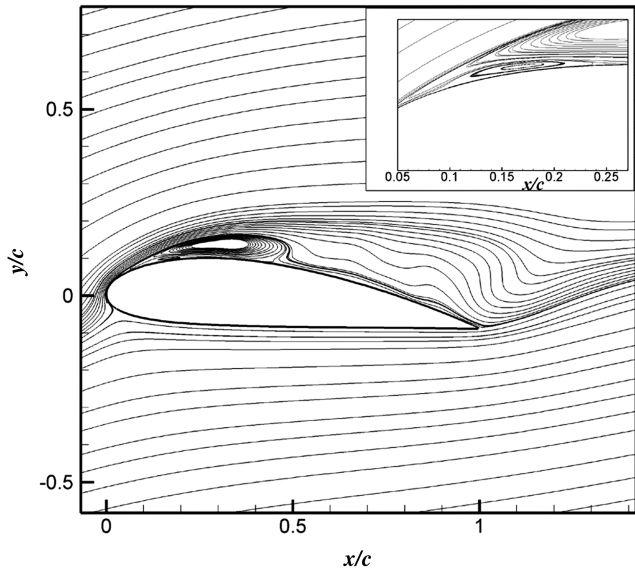
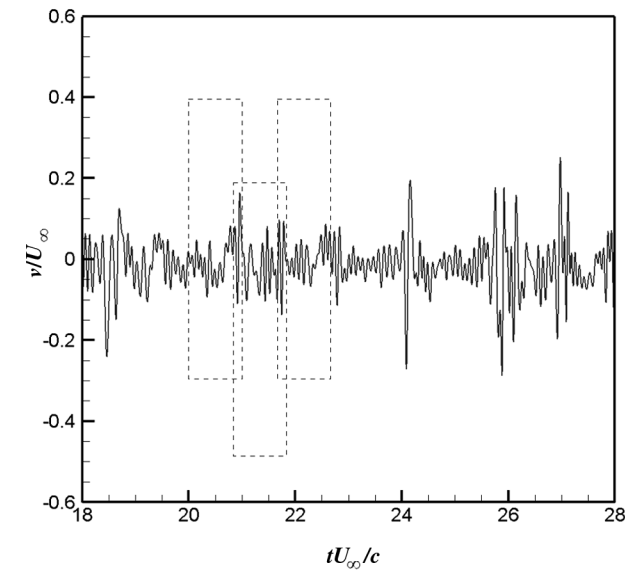


Fig. 6 Time-averaged streamlines of the uncontrolled flow.

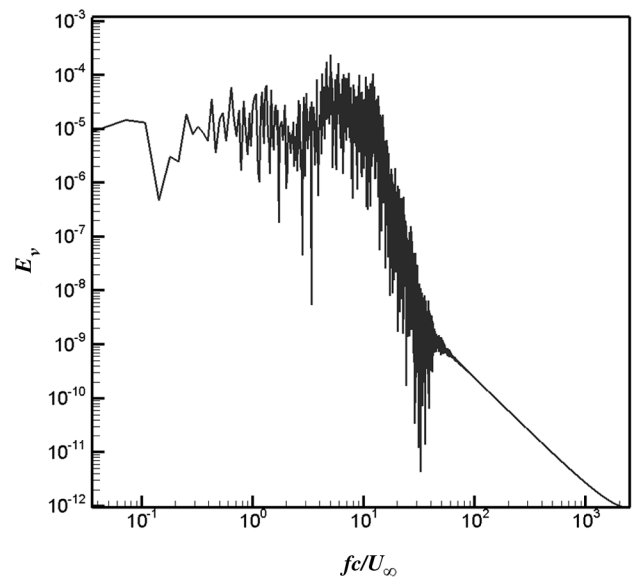
Using the same techniques (PDF-based as well as ensemble averaged spectrum), the separation bubble and wake frequencies have been identified as $f_{sep}^+ \approx 2$ and $f_{wake}^+ \approx 1$, respectively, and these are shown in Fig. 8. Note that due to the stochastic nature of the flow, the values calculated are approximate involving an uncertainty of around 2–10%. This uncertainty was estimated by determining the variation based on different window sizes with the current average value.

B. Zero-Net Mass-Flux Forcing

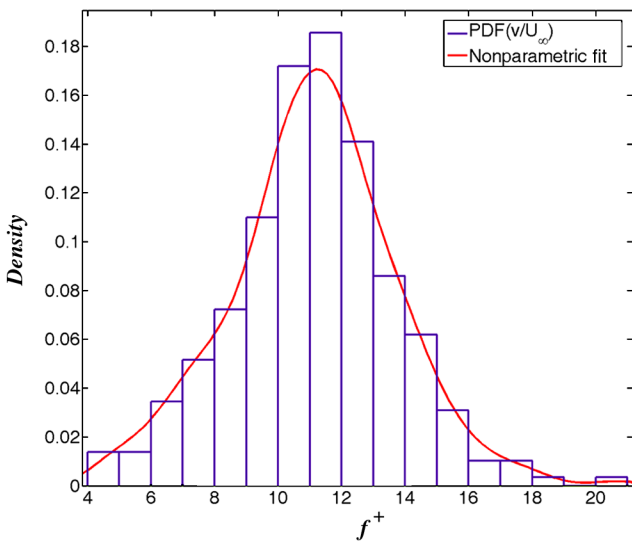
Because the characteristic frequencies for this flow range from 1.0–12.0, the frequencies of the forced flow cases (listed in Table 1) have been chosen such as to encompass this range. Cases 1–6 are chosen such that $f_j^+ = m \cdot f_{sep}^+$, where $m = 1/4, 1/2, 3/4, 1, 3/2,$ and 2. Note that although these cases have been chosen primarily based on f_{sep}^+ , they are not necessarily its sub- or superharmonic (e.g., cases 3 and 5). It should also be mentioned that since $f_{sep}^+ \approx 2 \cdot f_{wake}^+$, the forcing frequencies in the current cases can also be related to f_{wake}^+ . Cases 8–10 are chosen to be close to the shear layer frequency f_{shear}^+ . The effect of the location on forcing is examined by placing the ZNMF jet inside the separation bubble in cases 11 and 12. For all the cases, we choose $V_0/U_\infty = 0.1$ which leads to values of momentum



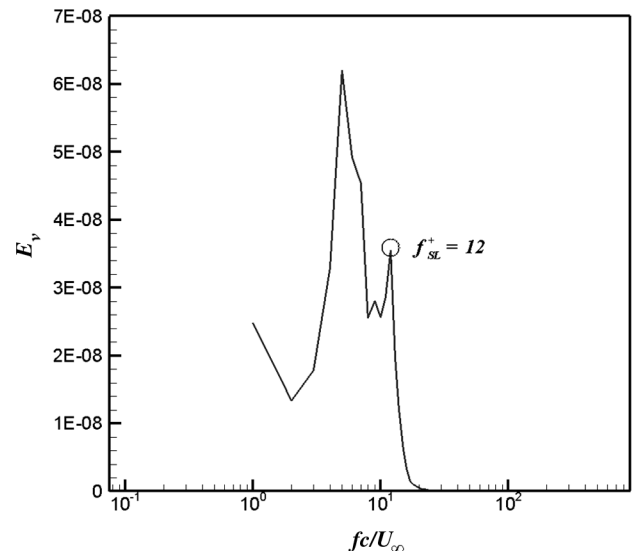
a)



b)



c)



d)

Fig. 7 a) Temporal variation of cross-stream velocity at probe locations $x^+ = 0.14$ and its b) corresponding power spectrum; c) PDF with a nonparametric fit, and d) averaged power spectrum identifying f_{sl}^+ .

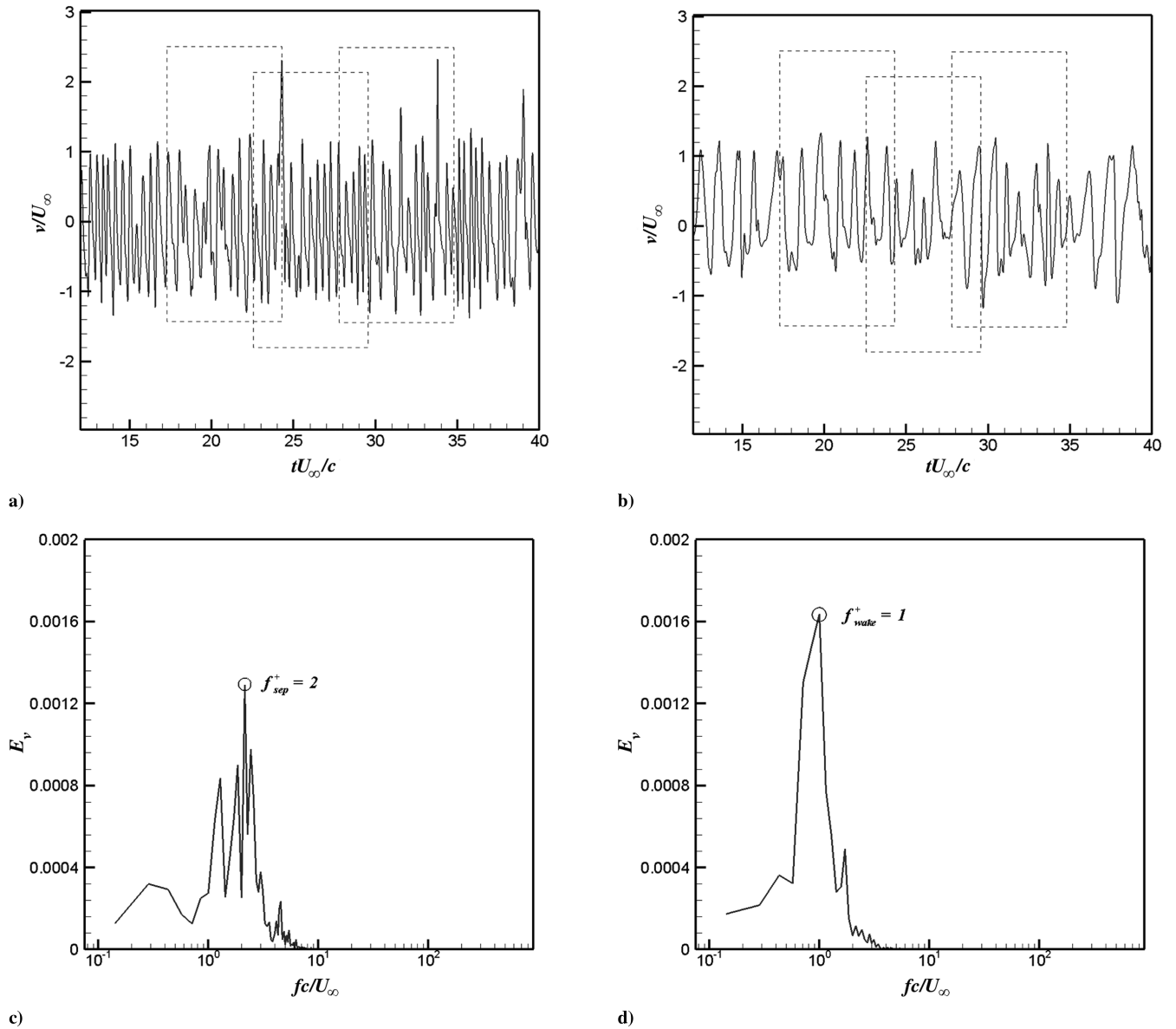


Fig. 8 Temporal variation of cross-stream velocity at probe locations a) $x^+ = 0.46$ and b) $x^+ = 1.22$. Corresponding power spectra showing the frequencies for c) separation bubble and d) wake.

coefficient, $C_\mu = 1.2 \times 10^{-4} - 1.9 \times 10^{-4}$. The momentum coefficient here is defined as

$$C_\mu = \rho w_J \int_0^{T/2} V_J(t)^2 dt / (0.5Tc(0.5\rho U_\infty^2))$$

where ρ is the density, T is the time period, $V_J(t)$ is the spatial-averaged velocity during the expulsion phase of a cycle, and w_J is the jet width [6].

The effect of forcing on the flowfield is demonstrated in Fig. 9 which shows the streamwise velocity contours as well as the velocity vectors. During peak expulsion it can be clearly seen that the boundary layer formed on the airfoil surface in the proximity of the jet is thicker than during peak ingestion. This follows the characteristics of a synthetic jet adding or removing momentum to/from the external boundary layer via periodic forcing. The vector fields also show that the magnitude of the forcing is significantly lower than the incoming velocity.

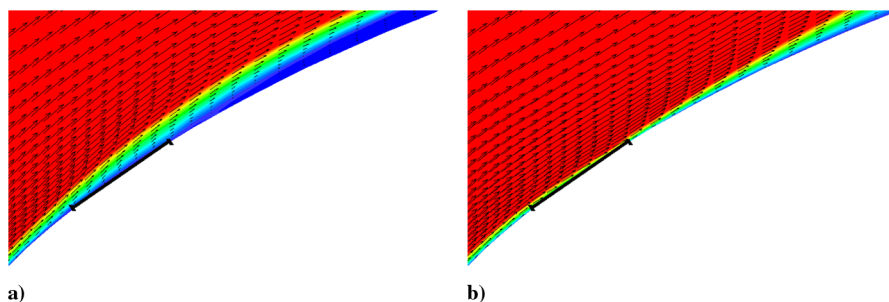


Fig. 9 Plots showing the streamwise velocity contour and velocity vectors for $f_j^+ = 2.0$, $x_j^+ = 0.024$ during peak a) expulsion b) ingestion in the proximity of the jet, represented by a solid line.

1. Forced Flow Characteristics

Figure 10 shows the instantaneous spanwise vorticity for all the forced flow cases at the same instant after forcing is initiated. The flow is analyzed after the initial transients related to the forcing are completely eliminated, which occurs after nearly five convective times or $5c/U_\infty$. The response of the separated flow to different forcing frequencies can be categorized in three categories as indicated in Table 1. In the first category, type I, which consists only of the low frequency $f_j^+ = 0.5$ case, we find that the forcing increases the size of the vortices formed in the separation region but otherwise has little effect on the angle at which the shear layer departs from the airfoil surface. The increase in the size of the vortices is a direct consequence of the flow adjusting to a larger time scale corresponding to the forcing.

The second category, type II, consists of cases where forcing ranges from $f_j^+ = 1.0$ to 6.0 , which is the range closely surrounding the f_{sep}^+ values of 2.0 . As can be seen from Figs. 10b–10f, the vortices in the separations region tend to remain attached over a greater length of the airfoil. What is noticeable is that as f_j^+ increases for these cases, there is a corresponding increase in the tendency or ability of the shear layer to produce discrete vortices. These vortices are able to convect downstream before merging with one another and eventually form the wake. This corresponds to the observations by Amitay and Glezer [43] that $\mathcal{O}(1)$ forcing causes formation of

vortical structures which scale with the separated region and results in a Coanda-like deflection of the shear layer toward the surface.

Figures 10h–10j correspond to the third category, type III, of cases. For these cases, forcing at frequencies which are close to the shear layer frequency leads to the formation of a number of small discrete vortices in the shear layer which merge to form a strong clockwise vortex which is larger in scale than the separation vortices seen for the unforced flow. The shear layer also seems to extend in a direction tangent to the direction of separation. Figure 10g shows that $f_j^+ = 6.0$ is a transitional case with behavior that has characteristics of both the second and third categories. On the other hand, placing the jet within the separation bubble does not seem to have a significant effect on the flow as seen in Figs. 10k and 10l. When compared with the flow pattern of the baseline case, see Fig. 5, the flow at $f_j^+ = 2.0$ and $x_j^+ = 0.070$ does not seem to exhibit effect of control, whereas at this location for $f_j^+ = 10.0$ the flow pattern seems very similar to when the jet is placed ahead of the separation bubble, Figs. 10i and 10l.

Mean streamlines seen in Fig. 11 show the effect of forcing on the mean separation bubble characteristics. It is seen that for the range of $f_j^+ = 1.0 - 4.0$ and $x_j^+ = 0.024$, the length of separation bubble is reduced by nearly 35–87%, respectively, while H_{sep} is reduced over the range of 70–90% for these cases. However, for the case with $f_j^+ = 0.5$, the length of the separation bubble remains unchanged

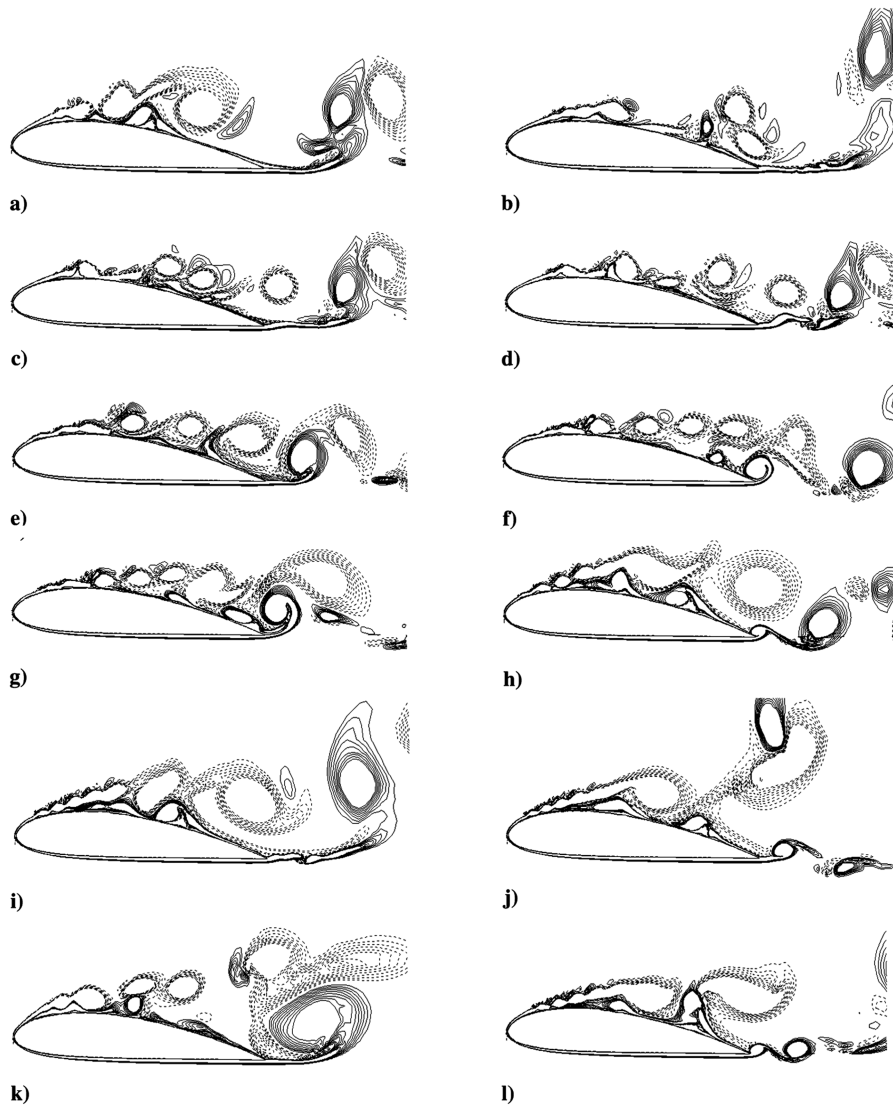


Fig. 10 Instantaneous spanwise vorticity showing the effect of forcing corresponding to a) $f_j^+ = 0.5, x_j^+ = 0.024$; b) $f_j^+ = 1.0, x_j^+ = 0.024$; c) $f_j^+ = 1.5, x_j^+ = 0.024$; d) $f_j^+ = 2.0, x_j^+ = 0.024$; e) $f_j^+ = 3.0, x_j^+ = 0.024$; f) $f_j^+ = 4.0, x_j^+ = 0.024$; g) $f_j^+ = 6.0, x_j^+ = 0.024$; h) $f_j^+ = 8.0, x_j^+ = 0.024$; i) $f_j^+ = 10.0, x_j^+ = 0.024$; j) $f_j^+ = 12.0, x_j^+ = 0.024$; k) $f_j^+ = 2.0, x_j^+ = 0.070$; and l) $f_j^+ = 10.0, x_j^+ = 0.070$ as compared to the baseline case shown in Fig. 5.

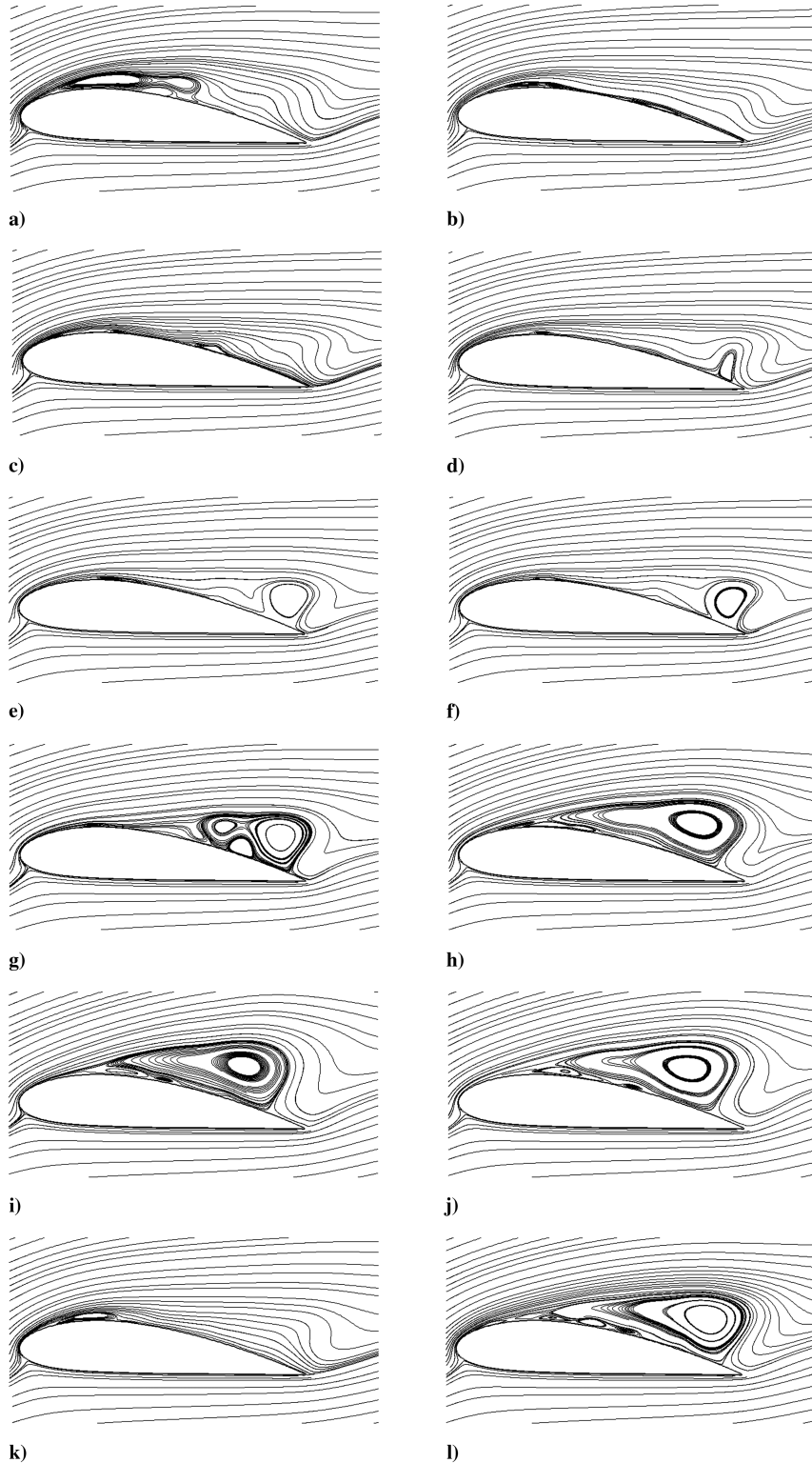


Fig. 11 Time-averaged streamlines showing the effect of forcing corresponding to a) $f_j^+ = 0.5$, $x_j^+ = 0.024$; b) $f_j^+ = 1.0$, $x_j^+ = 0.024$; c) $f_j^+ = 1.5$, $x_j^+ = 0.024$; d) $f_j^+ = 2.0$, $x_j^+ = 0.024$; e) $f_j^+ = 3.0$, $x_j^+ = 0.024$; f) $f_j^+ = 4.0$, $x_j^+ = 0.024$; g) $f_j^+ = 6.0$, $x_j^+ = 0.024$; h) $f_j^+ = 8.0$, $x_j^+ = 0.024$; i) $f_j^+ = 10.0$, $x_j^+ = 0.024$; j) $f_j^+ = 12.0$, $x_j^+ = 0.024$; k) $f_j^+ = 2.0$, $x_j^+ = 0.070$; and l) $f_j^+ = 10.0$, $x_j^+ = 0.070$ as compared to the baseline case shown in Fig. 6.

and there is an increase in its height by nearly 21% as seen in Fig. 11a. This increase is commensurate with the larger vortices that are formed due to the lower-frequency forcing. On the other hand, forcing at $f_j^+ = 8.0$, 10.0, and 12.0 increases the size of the recirculation region, which now extends over most of the surface of the airfoil due to the presence of larger separating vortices, seen in Figs. 11h–11j. Note that $f_j^+ = 3.0$ and 4.0 show hints of trailing-edge separation which becomes more prominent at the frequency of

$f_j^+ = 6.0$, see Fig. 11g, before fully manifesting as a large scale separation at higher frequencies.

Changing the location to $x_j^+ = 0.070$ at $f_j^+ = 2.0$ leads to a 40% reduction in L_{sep} compared to the baseline case, while there is a corresponding decrease in H_{sep} by nearly 57%, as shown in Fig. 11k. This suggests that forcing at frequencies close to f_{sep}^+ ahead of the unstable shear layer generates a better response in controlling separation than placing the jet inside the separation bubble. It might

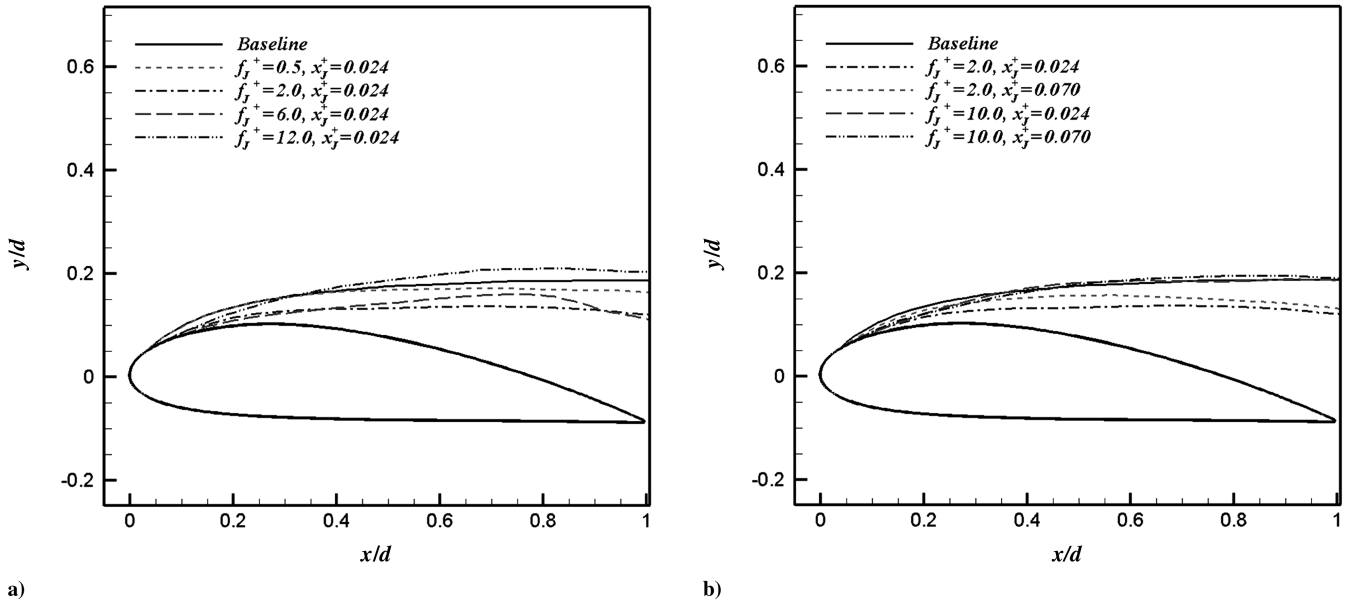


Fig. 12 Comparison of the time-averaged separating vortex trajectories for various a) frequencies and b) locations.

also be possible that placement inside the separation bubble requires a higher momentum coefficient to generate a similar response. However, this possibility has not been explored for the current study. On the other hand, high-frequency forcing at the same location at $f_j^+ = 10.0$, shown in Fig. 11i, has a similar behavior to when the actuator is placed ahead of the separation bubble, as seen in Fig. 11i.

The degree to which the vortices formed in the separation region are brought closer to the airfoil surface also provides insight into aspects of separation control for various cases. The mean vortex trajectories followed by the separating vortices, shown in Figs. 12a and 12b, give us an overview of this aspect of separation control. These trajectories are calculated as regions with highest vorticity concentration along the x direction, on the top surface of the airfoil. For $f_j^+ = 2.0$, $x_j^+ = 0.024$, the discrete vortices are usually found to be smaller as seen from the concentration of vorticity on the top of the airfoil (see Fig. 10d), and they tend to move closer to the airfoil surface, as seen in Fig. 12a. This is true for most of the cases in the response category type II. On the other hand, at $f_j^+ = 0.5$, $x_j^+ = 0.024$, the performance deteriorates in this regard because the vortices travel farther from the airfoil surface with a trajectory that is very similar to that of the baseline case. At higher frequencies the vortices tend to follow an initial straight path and therefore detach early from the airfoil surface with a wider spread as seen for $f_j^+ = 8.0$ and 12.0 , $x_j^+ = 0.024$ in Fig. 12a. Figure 12b shows that placing the jet inside the separation bubble and operating it at $f_j^+ = 2.0$ does not improve the performance compared to the standard upstream placement. On the other hand, operating at higher frequencies, that is, $f_j^+ = 10.0$, does not change these trajectories irrespective of the location.

Based on these observations, a clearer picture emerges regarding the flow response at the higher frequencies in the current configuration. For the baseline uncontrolled flow, the shear layer evolves in the vicinity of the separation region and its dynamics are substantially modified by its proximity to the surface. In particular, formation of the separation bubble vortices allows for mixing of high momentum outer flow into the separated region and tends to mitigate to some extent the effect of the adverse pressure gradient, consequently moving the shear layer closer to the airfoil surface. This overall behavior is further enhanced when the forcing frequency is in the vicinity of the natural separation bubble frequency and leads to further reduction in separation. In contrast, when the shear layer is forced at or close to its natural frequency it enhances the shear layer's ability to evolve relatively independent of the dynamics of the separation region. Consequently, the shear layer moves in an almost straight line from the point of separation, resulting in a larger

separation region over the airfoil. Thus, even though the effect of forcing at higher frequency is not the desired one in the current context, the effect is nevertheless interesting because it provides further insights into both the uncontrolled and controlled flow cases. There is a possibility that high-frequency forcing elicits a response in the flow that is intrinsically three dimensional and can therefore not be captured correctly in the current 2-D simulations. However, the study of Kotapati [44] has shown that results from 2-D and 3-D simulations for high-frequency forcing are similar in this regard, which would tend to diminish this possibility.

It should also be recognized that in addition to the forcing frequency, jet location, jet momentum coefficient flow Reynolds number, and airfoil configuration also play a significant role in determining the effect of the jet on the external flow. Thus, it is possible that there might be situations where high-frequency forcing results in separation reduction. In fact, Amitay et al. [6] show that for their unconventional airfoil, the lift-to-drag ratio has a decreasing trend as the forcing frequency is increased past $F^+ \sim 1$ but shows higher values beyond $F^+ \sim 12$. In this context, while the results of the current computations are necessarily limited in terms of the parameter space, they would seem to confirm that the effect of forcing at different frequencies is sensitive to these other parameters. The simulations also suggest a flow behavior at high frequencies that has not been described before and this merits further study in the future.

The time-averaged pressure coefficient for the four representative control cases is compared with the baseline case in Fig. 13a. With the exception of the highest frequency case, the suction peaks for the controlled cases are higher than the baseline case. The suction side behavior of the case with $f_j^+ = 0.5$ remains similar to the baseline case. Overall, for the control case with $f_j^+ = 2$, $x_j^+ = 0.024$, smooth pressure recovery is obtained until the trailing edge. For the case with $f_j^+ = 12.0$ the suction peak is followed by a large plateau, extending from $x^+ \sim 0.2$ to nearly the trailing edge of the airfoil. The trailing edge shows higher pressure on the suction side in comparison to the baseline case. As can be seen for $f_j^+ = 6.0$, for nearly one-fourth of the chord from the leading edge the pressure recovery is similar to the $f_j^+ = 2.0$ case, while for the remaining length it tends toward $f_j^+ = 12.0$, clearly marking this case as transitional from lower to higher frequency condition.

Figure 13b compares the effects of actuator location on the pressure recovery. For $f_j^+ = 2.0$ moving the jet inside the separation bubble tends to decrease the suction peak and overall the recovery shows a similar trend to the baseline case. On the other hand, for higher frequencies the recovery does not vary much with the change of location.

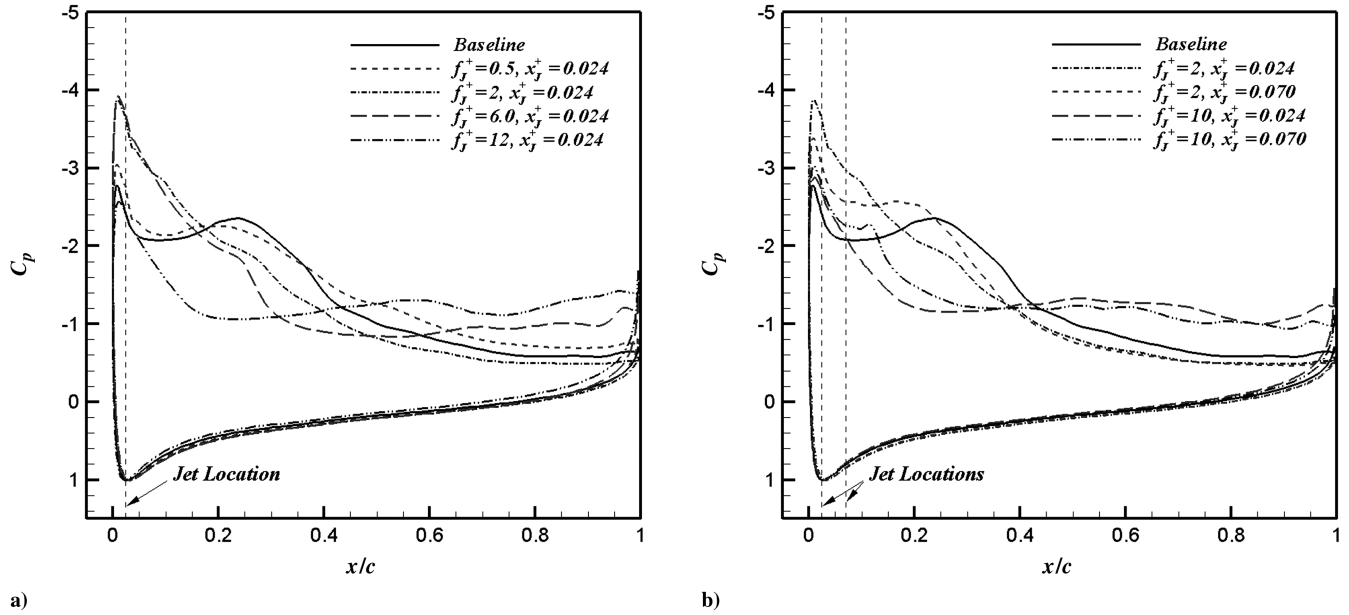


Fig. 13 Comparison of time-averaged pressure coefficient baseline and controlled cases for various a) frequencies and b) locations.

2. Effect of Forcing on Temporal Characteristics of Flow

It is known that the shear layer is able to lock on to the forcing frequency or its superharmonics, which is necessary for effective shear layer control [9]. Figures 14 and 15 show power spectra for the various forced cases, which allow us to examine the effect of forcing frequency on the temporal characteristics of the forced flow. These spectra have been offset in the vertical direction to separate them and make them easy to read. The shear layer, separation bubble, and wake probe locations, where the spectra are computed, are similar to the ones shown in Fig. 5a, with the exception of the separation bubble location which varies for different frequencies. These corresponding x^+ locations are provided in each of the spectral plots. The spectra are computed from the temporal variation of cross-stream velocity over 28 convective time intervals at the respective locations. As seen from the previous results the most effective forcing for reduction in the separation bubble size is when $f_j^+ = 2$, $x_j^+ = 0.024$. We find that for this case, the shear layer and the separation bubble show a distinct lock on to the forcing frequency as seen in Fig. 14c. The wake, however, shows a broad dominant peak around $f^+ = 1$, which indicates that the wake retains most of its natural dynamics. For $f_j^+ = 1$ (shown in Fig. 14b) and the rest of the type II cases we observe a similar behavior wherein the shear layer and separation bubble always lock onto the forcing frequency. On the other hand, forcing at lower frequency $f_j^+ = 0.5$, as seen in Fig. 14a, does not lead to any distinct lock on in any of the probed regions of the flow.

For $f_j^+ = 6.0$ and cases lying in the response category III with $f_j^+ > 6.0$, Figs. 14d–14f show that although the shear layer locks on to the forcing frequency, both the separation region and the wake exhibit virtually no response to the forcing. This clearly implies that the forcing is well outside the receptive range for these phenomena. Interestingly though, the separation region and wake show very similar power spectral shapes, indicating that these two regions have effectively merged and no longer show distinct dynamics. Furthermore, the dominant frequency in this region shifts to a lower value of about 0.8 for $f_j^+ = 6.0$ and 0.4–0.6 for $f_j^+ = 12.0$. This is consistent with the formation of large clockwise vortices on the suction surface resulting from the merger of many shear layer vortices. Thus, even though the high-frequency forcing does not couple directly with the separation bubble or the wake, its effect on these regions is quite substantial. Such a phenomenon is particularly interesting since ZNMF jets can also be used for virtual-aeroshaping effects [45,46]. It is important to emphasize that for virtual aeroshaping to occur, the actuation frequency and amplitude should be high enough such that there is an effective decoupling between the forcing and the wake instabilities, resulting in an interaction region

that is time invariant [10]. Our current forcing frequencies and amplitudes are not high enough to satisfy these conditions, and therefore the virtual-aeroshaping effects are not produced here.

If the actuation location is shifted to $x_j^+ = 0.070$, that is, downstream of the separation point, while forcing at $f_j^+ = 2.0$, the separation bubble appears to lock on to the forcing frequency as seen in Fig. 15a. However, unlike the case where the jet is placed ahead of the separation point, the shear layer exhibits a broader peak around the forcing frequency. This might indicate that the shear layer is unable to lock on to the forcing at all times. One possible reason could be insufficient forcing amplitude. Interestingly, unlike in the previous case with $f_j^+ = 2.0$, if the frequency is kept closer to the shear layer frequency at this location, then the flow exhibits patterns similar to forcing ahead of the separation point. Figure 15b shows that shear layer exhibits response to both the high forcing frequency and its superharmonics while the separation bubble and wake are not locked onto the forcing frequency.

In general we observe that varying the forcing frequency has a distinct effect on the dominant characteristics of the flow. Sinusoidal forcing near the natural separation bubble frequency ahead of the separation tends to modify both the shear layer and the separation bubble characteristics without having a significant effect on the wake. Thus, by locking onto the local instability of the flow it is possible to control the leading-edge separation. In addition, this instability is most receptive to forcing ahead of the separation as was also observed in an earlier study [31]. However, when forcing is applied at frequencies close to that of the shear layer, only the shear layer is able to lock on to the forcing, and this leads to global modification of the flow due to vortex merging in the separation region.

3. Aerodynamic Performance

The primary goal of the reducing separation over the airfoil is to recover good aerodynamic performance as measured by the lift and drag. Aerodynamic performance of the airfoil in response to forcing is examined here by comparing the averaged total lift-and-drag coefficients along with the lift-to-drag ratio. Figure 16a compares the drag coefficients to the baseline case. The percentage differences of individual control cases from the baseline case are listed in Table 1. It is found that frequencies closer to f_{sep}^+ show significant reduction in the drag with $f_j^+ = 2$, $x_j^+ = 0.024$ showing approximately a 39% decrease. The exception for these cases is forcing at $f_j^+ = 0.5$, $x_j^+ = 0.024$, which increases the drag by 13%. On the other hand, operating at higher forcing frequencies increases the drag by nearly

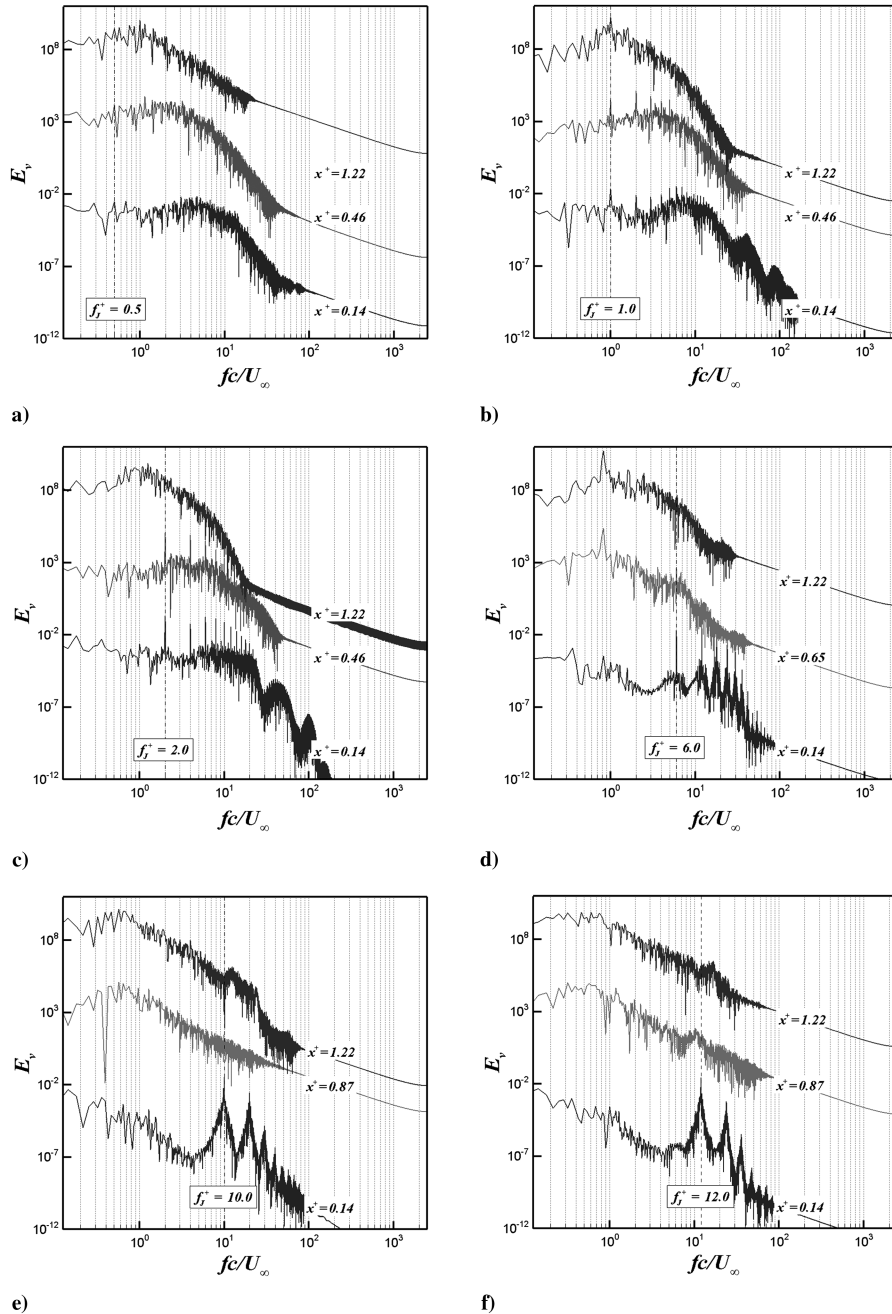


Fig. 14 Power spectra of the cross-stream velocity component corresponding to the shear layer (bottom), separation bubble (middle), and wake (top) for a) $f_j^+ = 0.5$, $x_j^+ = 0.024$; b) $f_j^+ = 1.0$, $x_j^+ = 0.024$; c) $f_j^+ = 2.0$, $x_j^+ = 0.024$; d) $f_j^+ = 6.0$, $x_j^+ = 0.024$; e) $f_j^+ = 10.0$, $x_j^+ = 0.024$; and f) $f_j^+ = 12.0$, $x_j^+ = 0.024$.

28–39%. However, there is no significant variation in the mean lift shown in Fig. 16b, where the $f_j^+ = 2, 3, 4,$ and 8 cases show a marginal increase in lift, while $f_j^+ = 10$ and 12 show a small decrease. Forcing at subharmonics of f_{sep}^+ increases the lift coefficient by nearly 8–10% over the baseline value. Comparison of the lift-to-drag ratio in Fig. 16c shows overall improvement in this quantity by nearly 64% for $f_j^+ = 2$, $x_j^+ = 0.024$ case while for $f_j^+ = 0.5$, the decrease is nearly 5%. The higher frequency cases show a decrease up to 34% in the lift-to-drag ratio. Interestingly, there is a direct correspondence between the type of response exhibited by the separated flow and the resultant aerodynamic performance. It is found that all the cases in type II exhibit an increase in the lift-to-drag ratio, whereas types I and II responses are accompanied by a decrease in this quantity.

Forcing inside the separation bubble for $f_j^+ = 2$ shows a slight decrease in lift while the drag is reduced by nearly 24%. On the other hand, the drag is increased by nearly 21% for $f_j^+ = 10$ at this

location. Figure 16b shows that the lift coefficient for this case does not change much in comparison to the baseline case.

IV. Conclusions

Detailed analysis of a poststall flow over a NACA 4418 airfoil at $Re_c = 40,000$ has been conducted using 2-D time-accurate simulations. The unforced separated flow is characterized by three distinct natural time scales corresponding to leading-edge shear layer, separation bubble, and the wake. Frequencies for sinusoidal forcing using a ZNMF actuator are chosen so as to cover the range of these natural frequencies of the flow. In addition to providing forcing ahead of the separation bubble, the effect of forcing location is also examined. It is found that forcing at or near the separation bubble frequency ahead of the separation point provides effective reduction in separation and a significant increase in the lift-to-drag ratio. When the excitation frequency is closer to the shear layer frequency, the

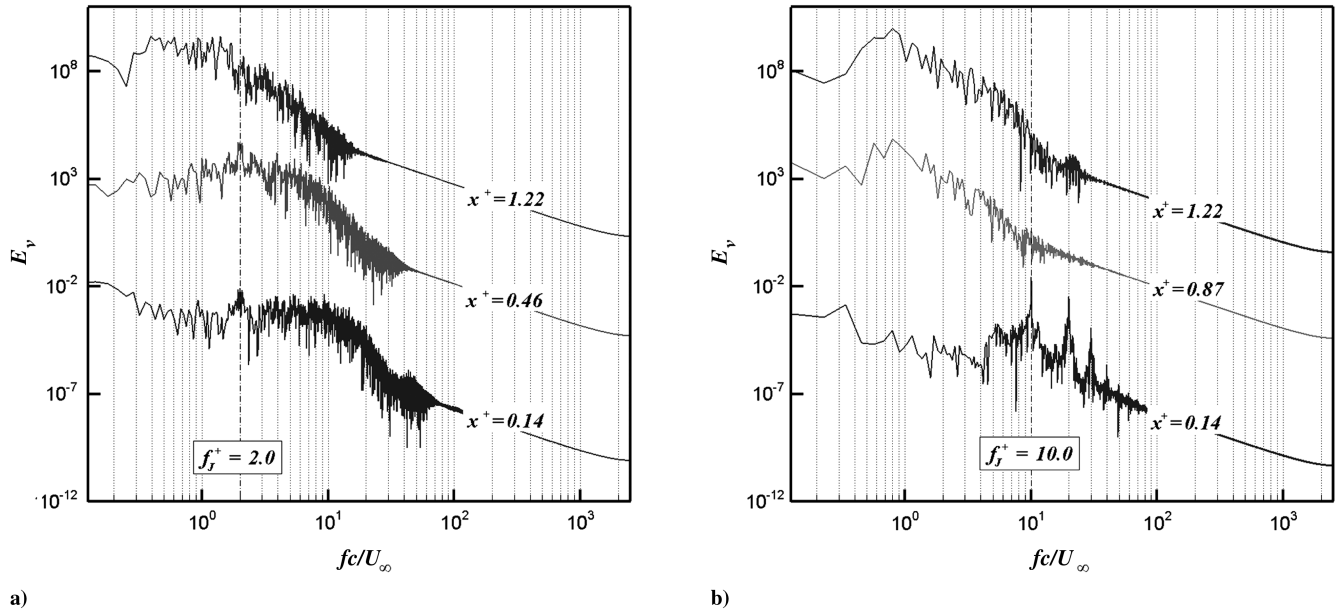


Fig. 15 Power spectra of the cross-stream velocity component corresponding to the shear layer (bottom), separation bubble (middle), and wake (top) for a) $f_j^+ = 2.0$, $x_j^+ = 0.070$; and b) $f_j^+ = 10.0$, $x_j^+ = 0.070$.

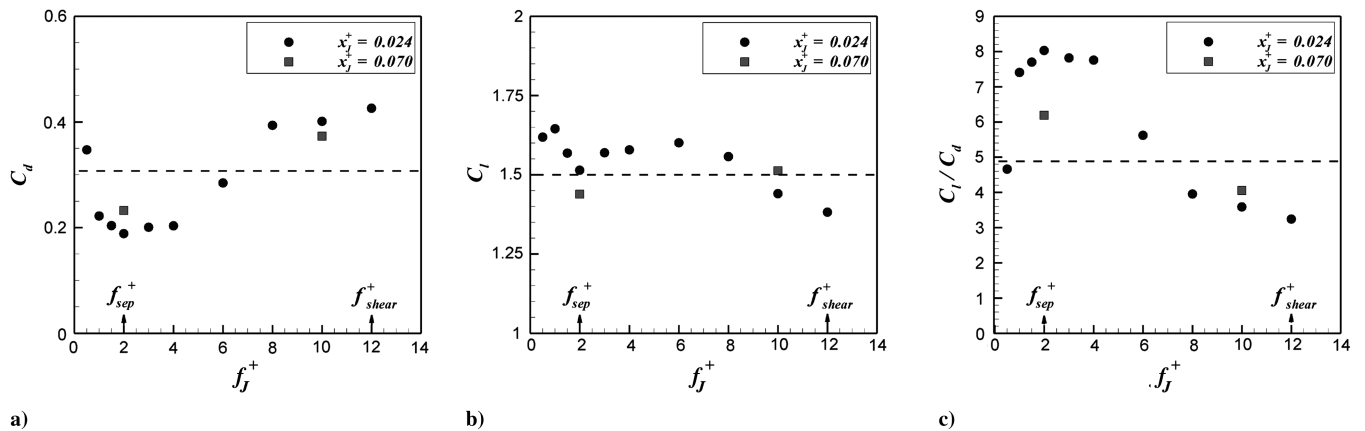


Fig. 16 Comparison of a) drag coefficient, b) lift coefficient, and c) lift-and-drag ratio for controlled cases as a function of frequency and location. The dashed lines indicate the baseline case value.

shear layer in the current case evolves independent of the dynamics of the separation bubble. The shear layer vortices merge to form large vortices in the separation region, and this tends to increase the size of the separation bubble and wake while reducing the frequency of vortex shedding. Thus, the end result of forcing at these high frequencies in terms of separation control is found to be unfavorable. It should, however, be noted that due to the limited parameter space addressed in the current study, it is difficult to make any general conclusions from the above observation. Nevertheless, the simulations do suggest a type of flow behavior at high frequencies that has not been described before and this merits further study. Placing the jet inside the separation bubble does not improve the lift-to-drag ratio. Overall, it is found that improvements in the aerodynamic performance are obtained primarily due to reduction in drag, whereas the effect on the lift coefficient is relatively small. Work is currently underway to study the effects of forcing based on the wake frequency. In addition, 3-D studies at higher angles of attack are also being carried out.

Acknowledgments

This work is supported by the U.S. Air Force Office of Scientific Research Grants (FA9550-05-0169 for R.M. and FA9550-05-0093

for L.C.). The authors are thankful to Reza Ghias for useful discussions and inputs on the compressible solver.

References

- [1] Hsiao, F., Liu, C.F., and Shyu, J.-Y., "Control of Wall-Separated Flow by Internal Acoustic Excitation," *AIAA Journal*, Vol. 28, No. 8, 1990, pp. 1440–1446.
doi:10.2514/3.25236
- [2] Seifert, A., Darabi, A., and Wygnanski, I., "Delay of Airfoil Stall by Periodic Excitation," *Journal of Aircraft*, Vol. 33, No. 4, 1996, pp. 691–698.
doi:10.2514/3.47003
- [3] Zaman, K., Bar-Sever, A., and Mangalam, S., "Effect of Acoustic Excitation on the Flow Over a Low-Re Airfoil," *Journal of Fluid Mechanics*, Vol. 182, Sept. 1987, pp. 127–148.
doi:10.1017/S0022112087002271
- [4] Seifert, A., Eliahu, S., Greenblatt, D., and Wygnanski, I., "Use of Piezoelectric Actuators for Airfoil Separation Control," *AIAA Journal*, Vol. 36, No. 8, 1998, pp. 1535–1537.
doi:10.2514/2.549
- [5] Seifert, A., and Pack, L., "Oscillatory Control of Separation at High Reynolds Numbers," *AIAA Journal*, Vol. 37, No. 9, 1999, pp. 1062–1071.
doi:10.2514/2.834

- [6] Amitay, M., Smith, D., Kibens, V., Parekh, D., and Glezer, A., "Aerodynamics Flow Control Over an Unconventional Airfoil Using Synthetic Jet Actuators," *AIAA Journal*, Vol. 39, No. 3, 2001, pp. 361–370.
doi:10.2514/2.1323
- [7] Amitay, M., Smith, B., and Glezer, A., "Aerodynamic Flow Control Using Synthetic Jet Technology," AIAA Paper 98-0208, 1998.
- [8] Glezer, A., and Amitay, M., "Synthetic Jets," *Annual Review of Fluid Mechanics*, Vol. 34, Jan. 2002, pp. 503–529.
doi:10.1146/annurev.fluid.34.090501.094913
- [9] Wu, J.-Z., Lu, X., Denny, A., Fan, M., and Wu, J.-M., "Post-Stall Flow Control on an Airfoil by Local Unsteady Forcing," *Journal of Fluid Mechanics*, Vol. 371, Sept. 1998, pp. 21–58.
doi:10.1017/S0022112098002055
- [10] Glezer, A., Amitay, M., and Honohan, A., "Aspects of Low- and High-Frequency Actuation for Aerodynamic Flow Control," *AIAA Journal*, Vol. 43, No. 7, 2005, pp. 1501–1511.
doi:10.2514/1.7411
- [11] Pack, L. G., Schaeffler, N. W., Yao, C.-S., and Seifert, A., "Active Control of Flow Separation from the Slat Shoulder of a Supercritical Airfoil," AIAA Paper 2002-3156, 2002.
- [12] Tian, Y., Cattafesta, L., and Mittal, R., "Adaptive Control of Separated Flow," AIAA Paper 2006-1401, 2006.
- [13] Yehoshua, T., and Seifert, A., "Active Boundary Layer Tripping Using Oscillatory Vorticity Generator," *Aerospace Science and Technology*, Vol. 10, No. 3, 2006, pp. 175–180.
doi:10.1016/j.ast.2005.10.007
- [14] Raju, R., Mittal, R., Gallas, Q., and Cattafesta, L., "Scaling of Vorticity Flux and Entrance Length Effects in Zero-Net Mass-Flux Devices," AIAA Paper 2005-4751, 2005.
- [15] Greenblatt, D., and Wygnanski, I., "Effect of Leading Edge Curvature on Airfoil Separation Control," *Journal of Aircraft*, Vol. 40, No. 3, 2003, pp. 473–481.
doi:10.2514/2.3142
- [16] Mittal, R., and Kotapati, R., "Resonant Mode Interaction in a Canonical Separated Flow," *Proceedings of the Sixth IUTAM Symposium on Laminar-Turbulent Transitions*, Springer, New York, 2006, pp. 341–348.
- [17] Roshko, A., "On the Development of Turbulent Wakes from Vortex Sheets," NACA Rept. 1191, 1954.
- [18] Ho, C. M., and Huerre, P., "Perturbed Free Shear Layers," *Annual Review of Fluid Mechanics*, Vol. 16, Jan. 1984, pp. 365–424.
doi:10.1146/annurev.fl.16.010184.002053
- [19] Kotapati, R., Mittal, R., Marxen, O., Ham, F., and Yo, D., "Numerical Simulations of Synthetic Jet Based Separation Control in a Canonical Separated Flow," AIAA Paper 2007-1308, 2007.
- [20] Bar-Sever, A., "Separation Control on an Airfoil by Periodic Forcing," *AIAA Journal*, Vol. 27, No. 6, 1989, pp. 820–821.
doi:10.2514/3.10184
- [21] Darabi, A., and Wygnanski, I., "On the Transient Process of Flow Reattachment by External Excitation," AIAA Paper 2002-3163, 2002.
- [22] Funk, R., Parekh, D., Crittenden, T., and Glezer, A., "Transient Separation Control Using Pulse Combustion Actuation," AIAA Paper 2002-3166, 2002.
- [23] Margalit, S., Greenblatt, D., Seifert, A., and Wygnanski, I., "Active Flow Control of a Delta Wing at High Incidence Using Segmented Piezoelectric Actuators," AIAA Paper 2002-3270, 2002.
- [24] Ravindran, S. S., "Active Control of Flow Separation Over an Airfoil," NASA TM-209838, 1999.
- [25] Seifert, A., Bachar, T., Koss, D., Shephelovich, M., and Wygnanski, I., "Oscillatory Blowing: A Tool to Delay Boundary-Layer Separation," *AIAA Journal*, Vol. 31, No. 11, 1993, pp. 2052–2060.
doi:10.2514/3.49121
- [26] Wygnanski, I., "Some New Observations Affecting the Control of Separation by Periodic Forcing," AIAA Paper 2000-2314, 2000.
- [27] Gilarranz, J. L., and Rediniotis, O. K., "Compact, High-Power Synthetic Jet Actuators for Flow Separation Control," AIAA Paper 2001-0737, 2001.
- [28] Greenblatt, D., and Wygnanski, I., "Parameters Affecting Dynamic Stall Control by Oscillatory Excitation," AIAA Paper 99-3121, 1999.
- [29] Pack, L., and Seifert, A., "Dynamics of Active Separation Control at High Reynolds Numbers," AIAA Paper 2000-0409, 2000.
- [30] Mittal, R., Kotapati, R., and Cattafesta, L., "Numerical Study of Resonant Interactions and Flow Control in a Canonical Separated Flow," AIAA Paper 2005-1261, 2005.
- [31] Kotapati, R., Mittal, R., and Cattafesta, L., "Numerical Experiments in Synthetic Jet Based Separation Control," AIAA Paper 2006-0320, 2006.
- [32] Zaman, K., and Culley, D., "A Study of Stall Control Over an Airfoil Using 'Synthetic Jets'," AIAA Paper 2006-98, 2006.
- [33] Ghias, R., Mittal, R., and Dong, H., "A Sharp Interface Immersed Boundary Method for Compressible Viscous Flows," *Journal of Computational Physics*, Vol. 225, No. 1, 2007, pp. 528–553.
doi:10.1016/j.jcp.2006.12.007
- [34] Ghias, R., Mittal, R., and Lund, T., "A Non-Body Conformal Grid Method for Simulation of Compressible Flows with Complex Immersed Boundaries," AIAA Paper 2004-0080, 2004.
- [35] Anderson, A. D., Tannehill, C. J., and Pletcher, R. H., *Computational Fluid Mechanics and Heat Transfer*, 2nd ed., Hemisphere Publishing Corporation, New York, 1984.
- [36] Leonard, B. P., "A Stable and Accurate Convection Modelling Procedure Based on Quadratic Upstream Interpolation," *Computer Methods in Applied Mechanics and Engineering*, Vol. 19, No. 1, 1979, pp. 59–98.
doi:10.1016/0045-7825(79)90034-3
- [37] Kennedy, C. A., Carpenter, M. A., and Lewis, R. M., "Low-Storage, Explicit Runge-Kutta Scheme for the Compressible Navier-Stokes Equations," ICASE Rept. 99-22, 1999.
- [38] Gallas, Q., Holman, R., Nishida, T., Carroll, B., Sheplak, M., and Cattafesta, L., "Lumped Element Modeling of Piezoelectric-Driven Synthetic Jet Actuators," *AIAA Journal*, Vol. 41, No. 2, 2003, pp. 240–247.
doi:10.2514/2.1936
- [39] Gallas, Q., Holman, R., Raju, R., Mittal, R., Sheplak, M., and Cattafesta, L., "Low Dimensional Modeling of Zero-Net Mass-Flux Actuators," AIAA Paper 2004-2413, 2004.
- [40] Rumsey, C. L., Gatski, T. B., Sellers, W. L., III, Vatsa, V. N., and Viken, S. A., "Summary of the 2004 Computational Fluid Dynamics Validation Workshop on Synthetic Jets," *AIAA Journal*, Vol. 44, No. 2, 2006, pp. 194–207.
doi:10.2514/1.12957
- [41] Raju, R., "Scaling Laws and Separation Control Strategies for Zero-Net Mass-Flux Actuators," D.Sc. Thesis, Mechanical and Aerospace Engineering, The George Washington University, Washington, DC, 2008.
- [42] Mittal, R., and Balachandar, S., "Effect of Three-Dimensionality on the Lift and Drag of Nominally Two-Dimensional Cylinders," *Physics of Fluids*, Vol. 7, No. 8, 1995, pp. 1841–1865.
doi:10.1063/1.868500
- [43] Amitay, M., and Glezer, A., "Role of Actuation Frequency in Controlled Flow Reattachment Over a Stalled Airfoil," *AIAA Journal*, Vol. 40, No. 2, 2002, pp. 209–216.
doi:10.2514/2.1662
- [44] Kotapati, R., "On Synthetic Jets and Their Application to Separation Control in Canonical Airfoil Flows," D.Sc. Thesis, Mechanical and Aerospace Engineering, The George Washington University, Washington, D.C., 2008.
- [45] Mittal, R., and Rampugoon, P., "On the Virtual Aeroshaping Effect of Synthetic Jets," *Physics of Fluids*, Vol. 14, No. 4, 2002, pp. 1533–1536.
doi:10.1063/1.1453470
- [46] Amitay, M., Smith, B. L., and Glezer, A., "Aerodynamic Flow Control Using Synthetic Jet Technology," AIAA Paper 98-0208, 1998.

A. Plotkin
Associate Editor